The 2002 Brimacombe Memorial Lecture
Iron and Steel Society

Modeling of the Continuous Casting of Steel—Past, Present, and Future

BRIAN G. THOMAS

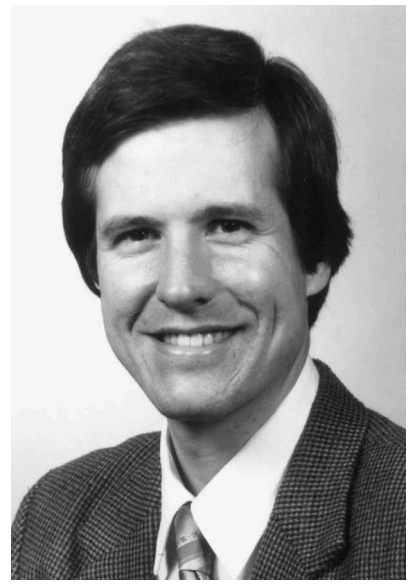

This lecture honoring Keith Brimacombe looks over the history, current abilities, and future potential of mathematical models to improve understanding and to help solve practical problems in the continuous casting of steel. Early finite-difference models of solidification, which were pioneered by Keith Brimacombe and his students, form the basis for the online dynamic models used to control spray water flow in a modern slab caster. Computational thermal-stress models, also pioneered by Brimacombe, have led to improved understanding of mold distortion, crack formation, and other phenomena. This has enabled process improvements, such as optimized mold geometry and spray-cooling design. Today, sophisticated models such as transient and multiphase fluid-flow simulations rival water modeling in providing insights into flow-related defects. Heat-flow and stress models have also advanced to yield new insights. As computer power increases and improvements *via* empirical plant trials become more costly, models will likely play an increasing role in future developments of complex mature processes, such as continuous casting.

The Brimacombe Memorial Lectureship was established in 1999 by the Process Technology Division of the Iron & Steel Society to honor Dr. J. Keith Brimacombe's outstanding accomplishments in the area of process metallurgy, his dedication to the steel industry, and his profound effect on people in the industry; and also to acquaint members, students, and engineers with the many exciting opportunities that exist in the area of process metallurgy and to inspire them to pursue careers in this field.

Brian G. Thomas is a professor of mechanical engineering at the University of Illinois and director of the Continuous Casting Consortium. He received his Bachelors of metallurgical engineering from McGill University in 1979 and Ph.D. in metallurgical engineering in 1985 from the University of British Columbia. In between, he worked in the Materials Research Department of Algoma Steel (Sault Ste. Marie, ON). His recent research efforts focus on the development and application of mathematical models of all aspects of the continuous casting of steel and related processes. Dr. Thomas has authored with co-workers over 150 technical publications on his research, which has been recognized with a Presidential Young Investigator Award from NSF, Outstanding Young Manufacturing Engineer Award from SME, Xerox Award for UIUC Faculty research, and more than ten best paper awards from AFS, AIME, ISS, TMS, CIM, and ASM International. He has participated in several short courses to transfer technology to industry, including the annual Brimacombe Continuous Casting Course.

I. FOREWORD

IT is a great privilege to present the second-ever J. Keith Brimacombe lecture at this 59th Electric Furnace Conference, the first of the Third Millennium. Professor Brimacombe was a giant in many fields. He also inspired many people, especially his students, including me. At the first Brimacombe lecture, last year, Indira Samarasekera gave an inspirational talk, which touched on many different facets of the research excellence that was the hallmark of this remarkable man's career.[1] Dr. Brimacombe left a legacy of leadership, knowledge, and genuine care for the people, which benefited the steel industry, the Iron and Steel Society, and many individuals here today. His technical contributions

spanned a wide range of materials engineering processes, including rotary kilns, injection, bath smelting, flash smelting, static and continuous casting, rolling, and microstructural engineering.

This year's lecture looks at the history, current state, and future prospects of the mathematical modeling of the continuous casting of steel. Of the many contributions that Dr. Brimacombe gave to process metallurgy, some of his best pioneering work was done to help create this field. He was a champion of modeling and he did much to improve its credibility and usefulness, through his example. This subject is also fitting, because his impact on the steel industry through short courses and publications on continuous casting made extensive use of the landmark results of his models. Indeed, he would have been the best choice to lecture on this topic, had he not suddenly left us in 1997. I am grateful to the organizers for asking me to give this lecture in an effort to continue his spirit.

II. INTRODUCTION

The continuous casting process and the digital computer appeared at about the same time. As casting technology and the striving for quality have advanced together, so too have computational models improved and, frequently, contributed to the former. This lecture will attempt to overview the past, present, and future of mathematical modeling of the continuous casting of steel. Many researchers have made significant contributions to this subject, starting with the early pioneers including Keith Brimacombe, I.V. Samarasekera, E. Mizikar, J. Szekely, K. Schwerdtfeger, T. Emi, and many others. As so much work has been done, it is impossible to give a comprehensive overview in this little time. I will instead provide a few examples which aim to illustrate the history of modeling and compare early and recent contributions. I will also highlight some of the work of Keith Brimacombe, who pioneered this field and to whom this lecture is dedicated.

III. THE PAST

In the early days of computational modeling, computer processors were barely as powerful as those in today's cell phones. Computers in the early 1970s were so slow that, for industrial applications, numerical methods were rivaled by analytical tools, such as Hill's integral profile method.[2] Design calculations, such as finding the metallurgical length of a casting machine, were performed exclusively using simple empirical equations[3,4] that could be solved by hand, such as

$$\text{Shell thickness} = K\sqrt{(\text{Distance/Casting speed})} \quad [1]$$

Here, K was found from costly plant trials ending in breakouts.

Keith Brimacombe was one of the first to envision the potential power of the new finite-difference and finite-element methods that had been originally been developed for the aerospace industry and were starting to expand into other areas. He realized that the powerful flexibility of these methods would "unleash the process engineer and mathematician from (the inherent limitations of) analytical solutions and create new opportunities for the analysis and understanding of processes."[5]

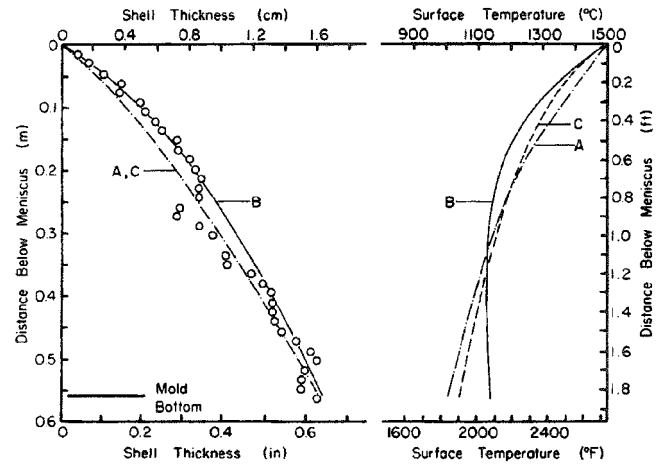

Fig. 1—Liquid pool and surface temperature profiles in the mold, comparing finite difference model (A) with analytical solution (C), and finite difference model (B) with shell thickness measured near a beam blank web.

A. *Shell Solidification Models*

In the late 1960s and early 1970s, Mizikar[6] and Lait *et al.*[7] pioneered the first finite-difference models of shell solidification. The models solve the following transient heat-conduction equation, subject to carefully chosen boundary conditions, by following a transverse slice though the shell as travels downward at the casting speed.

$$\rho\frac{\partial H}{\partial t} = \nabla \cdot k\nabla T \quad [2]$$

where ρ is the density (kg/m^3), H is the enthalpy (J/m^3), t is the time (s), k is the thermal conductivity, and T is the temperature ($^\circ$C).

Figure 1[8] shows typical results from such a model, with the shell-growth profile on the left-hand side and surface temperature on the right-hand side. At the same time, others, most notably J. Szekely, were making impressive demonstrations of computational modeling of other important phenomena, such as turbulent fluid flow in the nozzle,[9] thermal mixing in the mold,[10] and nozzle clogging.[11] These early modeling efforts were ground-breaking and foreshadowed the wide range of applications common today. But, they sometimes suffered from computational limitations.

Brimacombe championed the crucial knowledge-creation practice of combining experiments and models together: forcing the models to match reality through calibration and validation. For example, Figure 1[8] also includes a simulation (line A) to compare with an analytical solution[2] using the integral profile method (line C). More significantly, this figure also contains data points to compare the predictions with shell-thickness measurements, in this case, from beam blank sections, such as pictured in Figure 2.[8] The pioneering spirit for model validation in these early days is perhaps best epitomized by how these figures were obtained: by injecting radioactive gold tracer into the mold of an operating steel caster. Today, it is standard practice for all models to be tested rigorously using, first, analytical solutions (to validate the internal consistency of the model and mesh refinement) and, then, measurements from experiments or plant trials (to validate modeling assumptions, property data, and boundary conditions).

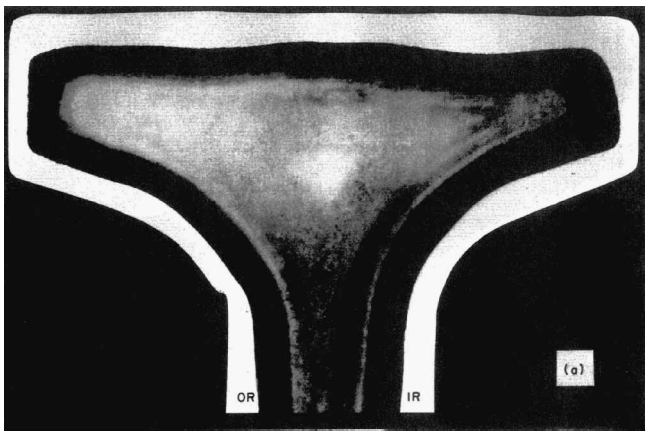

Fig. 2—Autoradiograph of a 30 × 45-cm, 0.21 pct C-steel beam blank treated with radioactive gold tracer at Algoma Steel showing shell thickness for Fig. 1.

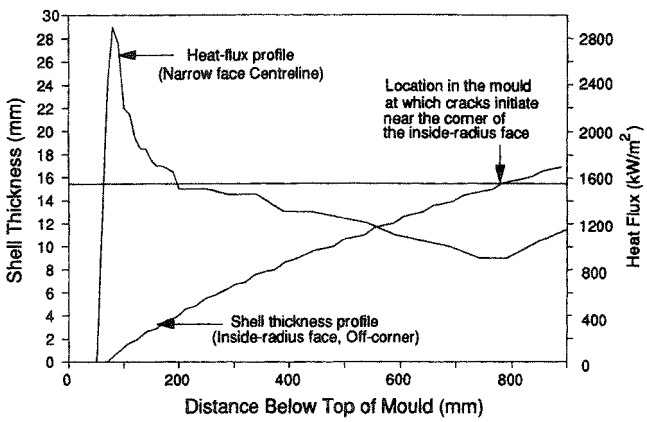

Fig. 3—Computed shell profile in a slab casting mold at the off-corner region of the wide face and axial heat-flux profile at the centerline of the narrow face.

Finally, Brimacombe showed that modeling computations are not simply academic curiosities, but can be used as powerful tools to solve practical problems in the real process. In a landmark article in 1976,[12] he showed how a one-dimensional (1-D) solidification model could accurately predict such useful information as

(1) the shell thickness at mold exit,
(2) the metallurgical length of the caster,
(3) the location down the caster where cracks initiate, and
(4) the cooling practice below the mold to avoid reheating cracks.

To achieve this, the model predictions must be combined together with knowledge gained from other sources. For example, Figure 3[13] compares a predicted shell-thickness profile with the closest distance (measured on a transverse section) between the strand surface and the tips of some short, subsurface longitudinal cracks. Metallurgical examination of the cracks revealed that they were "hot tears," which initiate at the solidification front, so the results indicate that the cracks formed near mold exit.

This methodology paved the way for a framework to diagnose and solve cracking problems in continuous casting, such as contained in the billet casting expert system

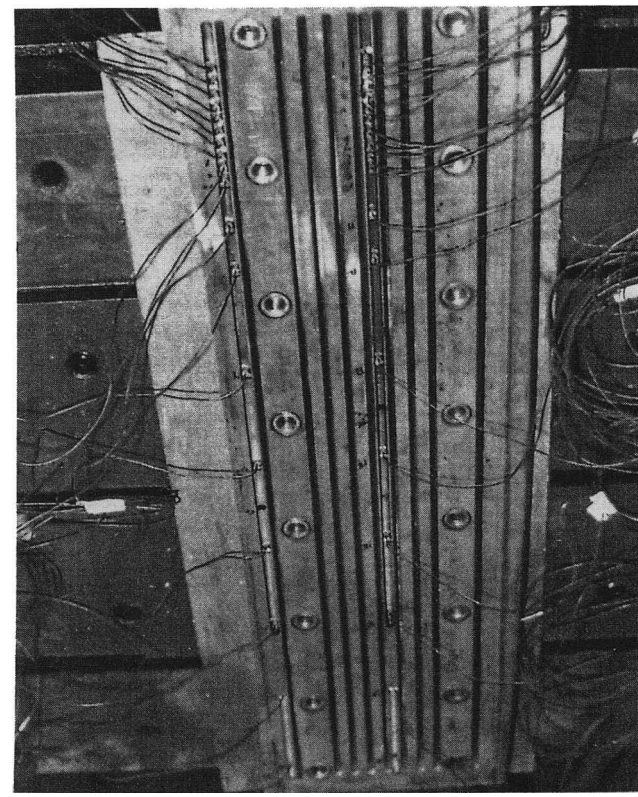

Fig. 4—Instrumented copper plate (narrow face) used to calculate heat flux in Fig. 3

CRACK-X, which Brimacombe developed later.[14] Today, refined versions of this original simple 1-D solidification model are standard tools on the desktop computers of many casting engineers and designers and can even run on a spreadsheet.[15] They are used for many purposes, such as trouble-shooting the cause of cracks, redesigning spray zones and support systems to accommodate increases in casting speed, or developing online control systems.

B. *Mold Thermal Distortion and Taper*

Brimacombe next pioneered the powerful combination of taking temperature measurements from thermocouples embedded in the copper mold wall and interpreting them with computational heat-flow model analysis. He showed how models can augment the clues hidden in the measurements, by converting the raw signals into more fundamental quantities, such as mold heat-flux profiles, that could better help to understand the process.

This important research practice has since been used to understand and solve many problems in continuous casting. For the example cracking problem mentioned in Figure 3, thermocouples were embedded into the mold wall, as shown in Figure 4.[13] The calculated increase in heat flux near mold exit provided an important clue that the narrow-face taper was too large and pushed against the shell, forming the observed off-corner depressions and cracks.[13] This conclusion could not have been drawn safely from the thermocouples alone, because the copper near the mold exit is usually hotter, due solely to the end of the water channel.

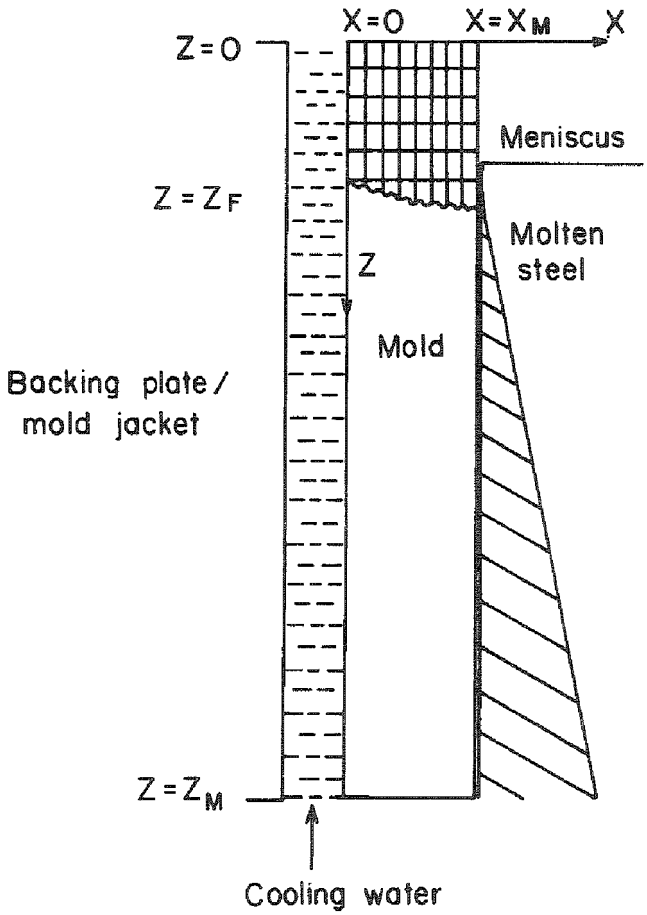

Fig. 5—Computational domain for 2-D finite difference model of heat conduction within the mold wall.

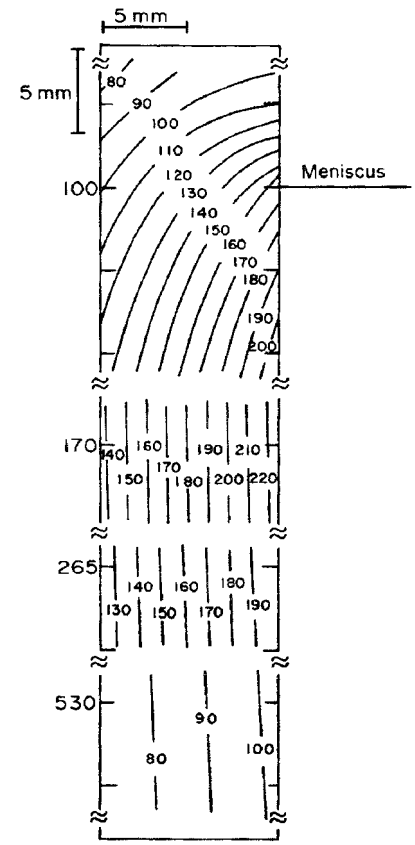

Fig. 6—Calculated temperature contours (9.5-mm billet mold wall of DLP Ag copper alloy casting high C steel at 2 m/min with 11 m/s water vel).

A two-dimensional (2-D) or three-dimensional (3-D) heat-flow model is needed to account for such mold geometry details.

This methodology was first applied by Samarasekera and Brimacombe in 1982. Figure 5[16] shows the 2-D grid of nodes and the rectangular domain they used to simulate heat conduction through the walls of a billet mold. Figure 6[16] shows the calculated temperature contours. This was the first work to show that due to axial heat flow, the maximum hot-face temperature develops slightly below the point of maximum heat flux, which is generally found at the meniscus. Of greater importance is the effect of this temperature profile on mold shape.

They next extended the state-of-the-art of mold analysis by inputting the calculated temperatures into a 3-D elastic-plastic finite-element model to calculate the distorted shape of a billet mold during operation. Figure 7[16] shows the calculated temperature profile down the mold, and Figure 8[17] shows the corresponding distorted shape profile, including the linear taper. The hottest part of the mold just below the meniscus expands to bulge away from the solidifying steel. Compared with the natural shrinkage of the shell away from the mold, which was calculated later,[17] a gap is predicted to form just below the meniscus. In practice, the shell bulges or wanders to touch one face or another, which gives rise to nonuniform heat transfer. The resulting temperature fluctuations in the shell cause stress, which leads to longitudinal cracks and other problems. To prevent this requires more taper in the upper part of the mold. Such modeling is ideally suited to optimize taper design. This led to the development of the parabolic taper, which is common practice in high-quality billet casting operations today.

C. *Thermal-Stress Analysis and Crack Formation*

Avoiding internal cracks was a critical challenge to early continuous casters, which is still very important today. Intuitively, internal crack formation depends on the thermal and mechanical stresses to which the shell is subjected. To help investigate the fundamentals of this problem, Brimacombe, with Grill and Weinberg[18] and Sorimachi,[19] applied the first finite-element thermal-stress models of solidification to understand the internal stress distribution in the solidifying steel strand below the mold.

They based their stress calculations on the temperature distributions, given in Figure 9,[12] which reveal increasing amounts of reheating for shorter spray-cooling zone lengths. They made a landmark qualitative insight: reheating of the strand surface below the end of the spray zones causes compression stresses there, which, in turn, force the subsurface into tension. This is shown in the calculated stress distribution in Figure 10.[19] The subsurface, where the solidification front is found, is very brittle because the liquid films between the dendrites are easily pulled apart. Thus, the reheating generates cracks at the solidification front.

With this knowledge, simple heat-transfer models could be applied to quantify the extent of reheating below the mold and to correlate this with cracks, such as halfway

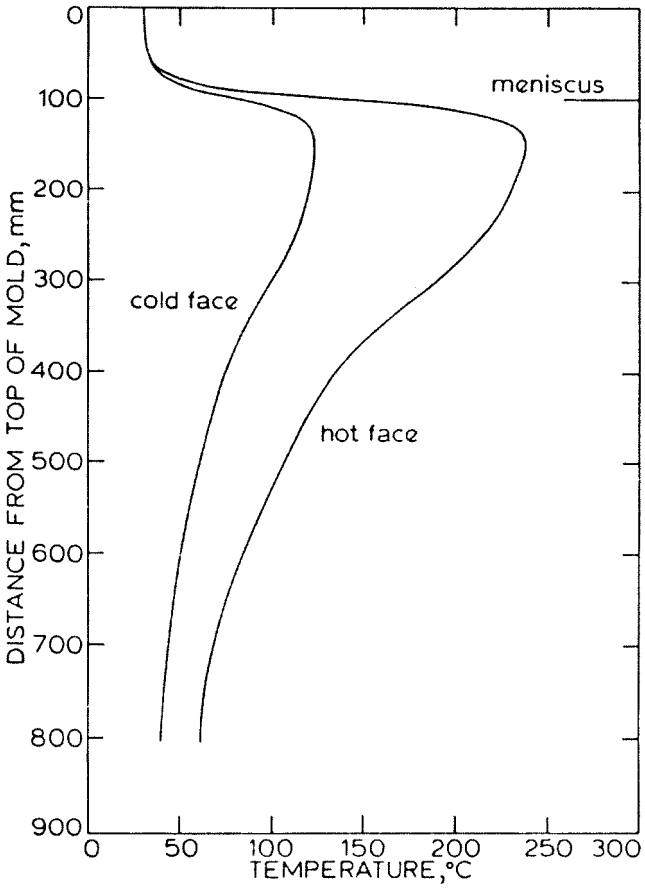

Fig. 7—Hot and cold face temperature profiles calculated in the billet mold wall (12.7-mm thick).

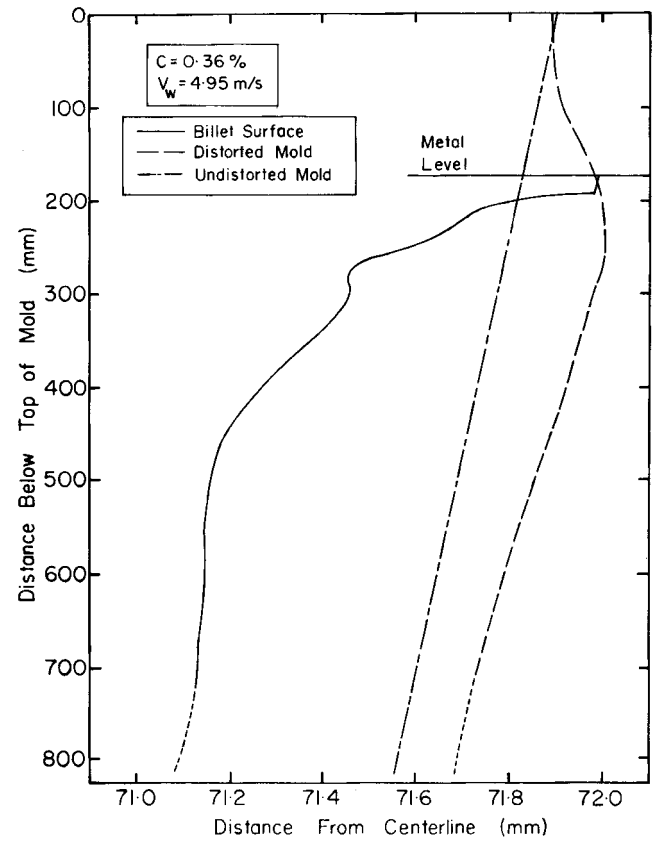

Fig. 8—Axial profile of billet and mold dimensions during operation showing the tendency surface to shrink away from mold wall.

cracks in billets. Criteria were published to choose a spray-zone length according to the casting speed and the allowable extent of reheating.[12]

The stress calculations used in this work were applied mainly to gain qualitative understanding of the evolution of regions of tension and compression within the strand as a function of processing conditions. This approach inspired subsequent modeling studies by others.[20,21,22] The quantitative use of stress models was not feasible in the early days, and is, indeed, still a challenge.

IV. THE COMPUTER REVOLUTION

As powerful computers now pervade almost every aspect of modern life, it is easy to forget how difficult computational modeling was in the early days, when Brimacombe and his colleagues were writing the first finite-difference models of continuous casting. After writing a program, it had to be typed onto punch cards, carried over to the computer building, and given to the computer operator. A simple compiler error would not be spotted until walking back to collect results the next day. A calculation that would today take only a few minutes on a personal computer might have been terminated by the mainframe operator before finishing, while burning up an entire year's computing allocation. Achieving meaningful results with these primitive tools makes the early modeling accomplishments all the more impressive.

The increase in application of models to the continuous casting of steel has coincided with tremendous increases in computing power. In the three decades since those first models, computer processor speed has increased more than 100,000-fold, with similar increases in storage capacity and dramatic decreases in cost. This has enabled the size and complexity of casting models to double every 1.5 years, as shown in Figure 11.[23] The mind-boggling magnitude of these advances can be illustrated by considering the impact that similar advances would have had on the auto industry. If car manufacturing had increased its speed, capacity, and cost efficiency to the same extent as computers have, then today's cars should carry more than 100,000 passengers, travel well over 1 million miles per hour, and cost less than 3 dollars to buy. The point is that our increasingly powerful computers should allow modeling to play an increasing role in future advances to high-technology processes such as the continuous casting of steel.

V. THE PRESENT

The tremendous increase in computer power is enabling better and faster models to contribute even more to continuous casting today. Yesterday's offline models can now run as real-time process-control models to implement knowledge directly into the caster. By making fewer simplifications and including more geometric details with better mesh refinement, today's offline models can be more accurate. We can now study more phenomena and their complex interactions together.

Lest we become too overconfident, however, it is

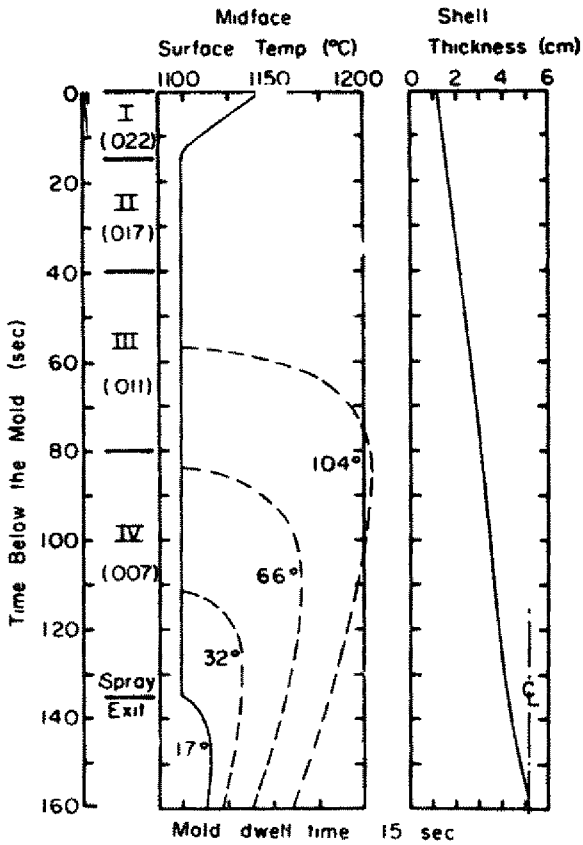

Fig. 9—Surface temperature profiles calculated along 10-cm square billet for different spray-zone lengths showing the extent of reheating and shell thickness profile.

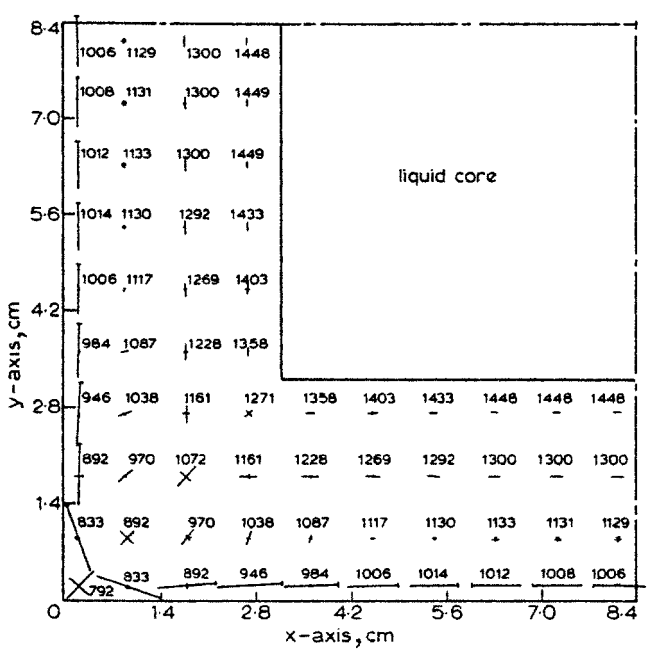

Fig. 10—Calculated stress distribution in solidifying shell (after 148 °C reheat). The temperature is typed in deg Celsius; crosses have lengths proportional to the principal stresses and the tic marks indicate compression.

important to recall exactly how complex the process of continuous casting really is. Figure 12 illustrates just some of

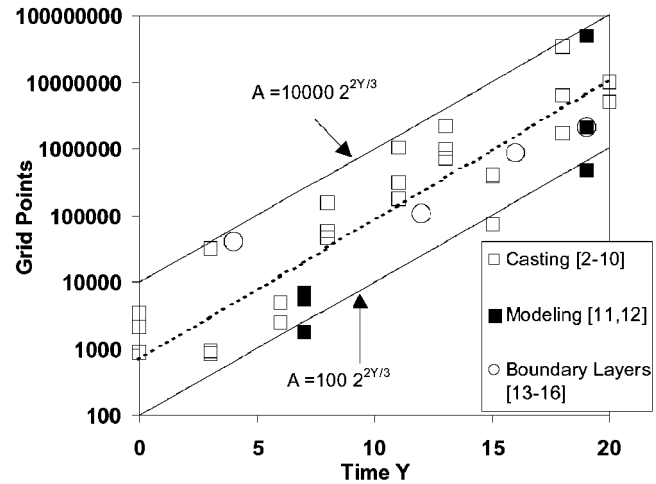

Fig. 11—Increase with year (from 1980 to 2000) of the three largest grid sizes used in computational models of casting processes.

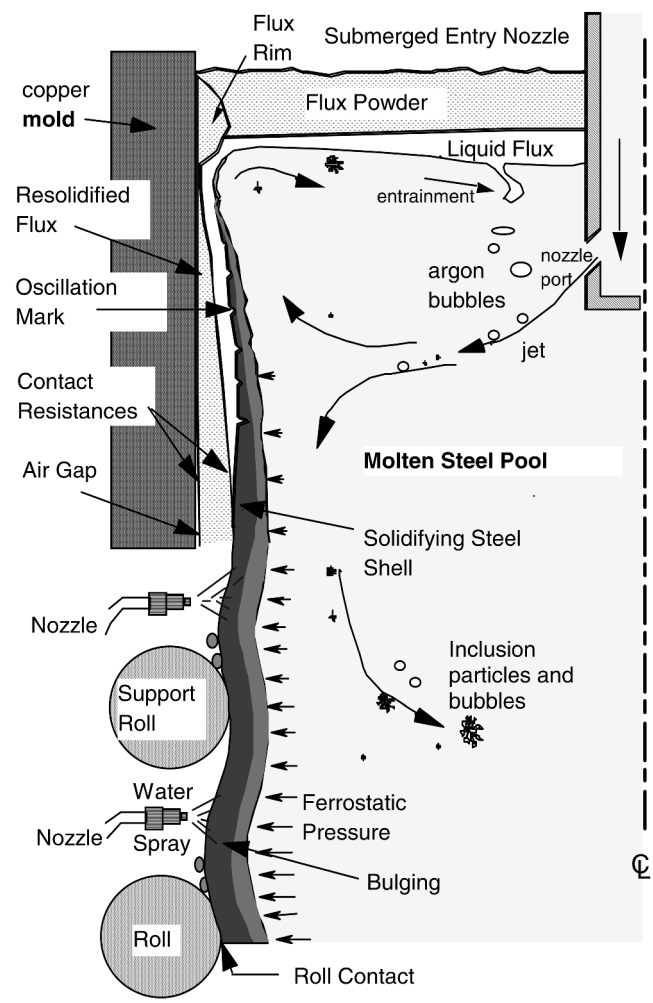

Fig. 12—Schematic of phenomena in the mold region of a steel slab caster.

the phenomena in the mold region that influence quality problems. They include the following steps:

(1) the complex-geometry nozzle ports direct the steel through the liquid pool contained within the curved sides of the dendrite walls;

(2) the turbulent jet, with its transient swirling eddies, flows according to the forces of momentum and, possibly, electromagnetics, buoyancy from gas bubbles, or natural convection;
(3) complex-shaped inclusion particles may collide with other particles, evolve in shape, and
  (a) float into the top slag to be removed (depending on the interfacial tension), or
  (b) become entrapped at the meniscus to form surface defects, or
  (c) move deep into the caster to form internal defects;
(4) gas bubbles from argon injection or reactions also are transported by the turbulent liquid and may coalesce or break up, collect inclusion particles, and, possibly, become entrapped as defects;
(5) dissolved solute and gases in the liquid can react according to nonequilibrium thermodynamics;
(6) the surface-contour shape is governed by the flow pattern, which, in turn, affects heat transfer in the slag layers, meniscus solidification, slag infiltration, and accompanying quality issues;
(7) entrainment of the slag layer to form mold slag inclusions will occur if the shear-flow velocity across the steel/slag interface is too high, depending on the viscosity, density, and interfacial tension;
(8) transient fluctuations and waves in the top-surface level are caused by the flow pattern, which create most surface defects at the meniscus by disrupting solidification and confusing the level control system;
(9) the superheat transported with the jet affects solidification hooks at the meniscus, shell thinning at the point of jet impingement, and precipitation of inclusions;
(10) the solidification microstructure depends on the nucleation, transport, and interaction of solid crystals, both in the flowing melt and against mold walls;
(11) solute transported with the flow governs both intermixing during a grade change and segregation on both microscopic and macroscopic scales;
(12) the meniscus region involves transient fluid, thermal, thermodynamic, and mechanical interactions between the solidifying steel, solid slag rim, infiltrating molten flux, liquid steel, powder layers, and inclusion particles;
(13) the interfacial gap between the shell and mold controls heat transfer according to the oscillation-mark depth, slag layer mass-transport and thermal properties, and possible air gaps;
(14) the steel shell solidifies and shrinks, according to the heat transfer, thermal contraction properties, phase transformations, and internal stresses;
(15) the mold walls and support rolls may distort, wear, and even crack;
(16) stress is generated within the solidifying steel shell, due to external forces (mold friction, bulging between the support rolls, withdrawal, and gravity), thermal strains, creep, and plasticity (which varies with temperature, grade, and cooling rate); and
(17) cracks may form, depending on the histories of temperature, stress, dendrite and grain microstructures, phase transformations, precipitate formation, segregation, and other complex phenomena.

Due to this staggering complexity, it will never be feasible to model all of these phenomena together with one model. Thus, the need for intelligent modeling assumptions, calibration with experiments, and the computational linking together of knowledge from different sources is as important today as it was before. At least, as computing power increases, modelers can expand their horizons a little to consider more of the phenomena important in the real continuous casting process. This section will touch on a few recent examples.

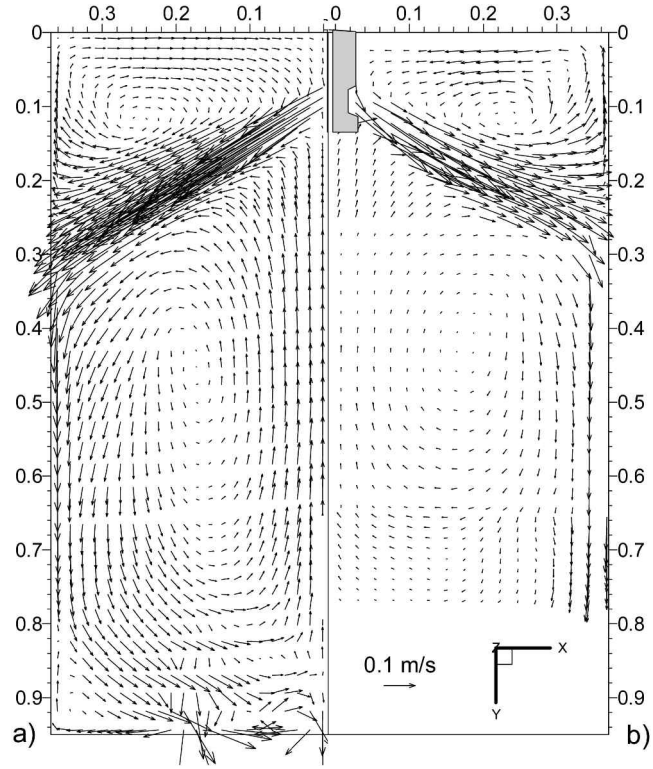

Fig. 13—Time average velocity vector plot of (a) LES2 simulation and (*b*) PIV measurement.

A. *Fluid Flow in the Mold*

In recent years, a great deal of advanced fluid-flow modeling has been done in the continuous casting of steel. Our recent review article on this subject includes over 100 such references.[24]

As an example, Figure 13[25] shows the time-averaged flow patterns in a closed-bottom water model of a typical slab-casting mold with a bifurcated nozzle. Velocity vectors are shown in at the center plane between the wide faces to indicate the local flow speed and direction. This figure compares results from two different state-of-the-art tools: large eddy simulation (LES) (on the left-hand side) and particle-image velocimetry (PIV) measurements (on the right-hand side). The PIV method works by illuminating tiny seed particles in the flow with a thin sheet of laser light and comparing the differences between two digital images of their positions taken only a microsecond apart, to calculate velocity vectors at each point. The results from hundreds of such image pairs are averaged to produce the flow field shown here. Both the model and measurement reveal the classic pair of simple recirculation zones in each half of the mold. Traditional K-ε models produce similar plots.[26]

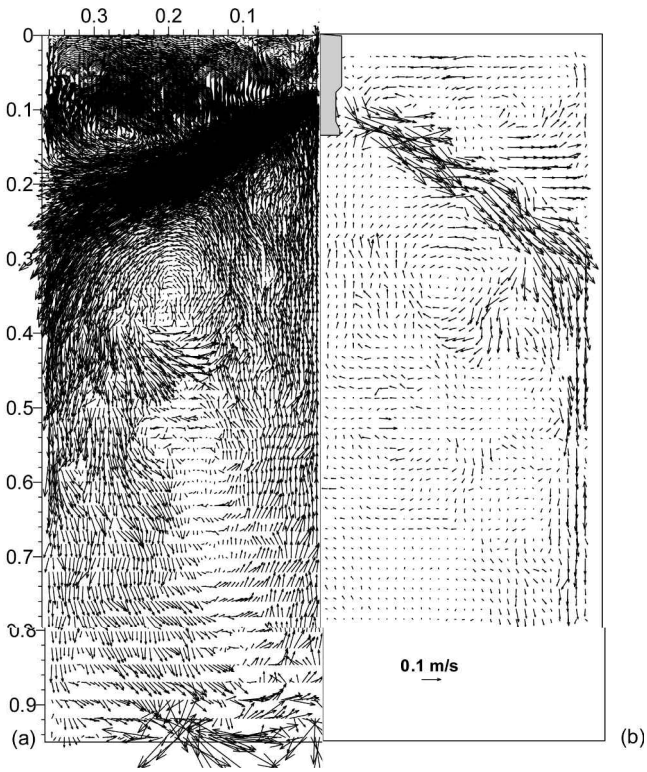

Fig. 14—Instantaneous velocity vector plot of (*a*) LES2 simulation and (*b*) PIV measurement.

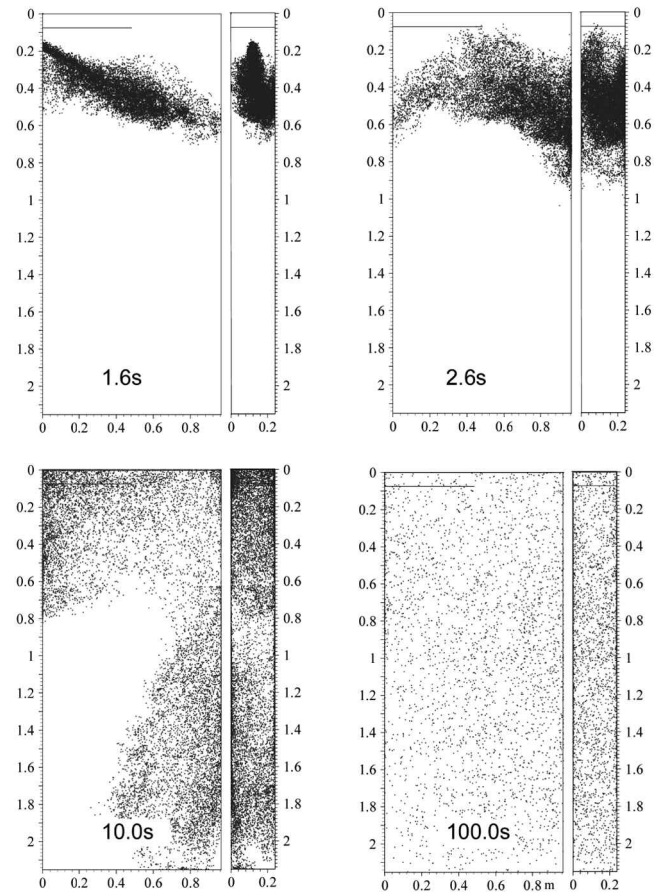

Fig. 15—Distribution of 15,000 particles at four instants after their injection through the nozzle port into the mold.

It has long been recognized that transient phenomena cause most of the quality problems in continuous casting. However, even finding the steady-state fluid-flow pattern has been a challenging task. This LES method can accurately capture the details of the transient motion, which is not possible with traditional steady K-ε models. It does this through brute computational force: solving the simple Navier–Stokes equations on a very fine mesh using small time steps and sophisticated parallel solvers, but without complex transport equations for turbulence. Figure 14[26] (left-hand side) shows an example snapshot of the transient flow field from the LES model. The mesh for this example contains over 1.5 million nodes and took 1 month of computer time. Only some of the velocity vectors are plotted to make the plot resolutions comparable to the PIV measurements (on the right-hand side). New features appear in the transient flow: the simple recirculation regions are, in reality, very complex and vary with time. Note that along the top surface, fast- and slow-moving flow structures alternate chaotically, sometimes producing time periods with a velocity much greater than the mean. This could be significant for slag emulsification and entrapment. Note in the lower roll, that a short-circuit flow appears in both the calculation and the measurement. This might be significant for particle motion.

Calculating an accurate flow pattern in the molten steel pool is interesting, but understanding its consequences on defect formation is more practical. The power of computational models is their ability to include other phenomena such as the convection of superheat, two-phase flow effects from argon gas injection, and the motion and entrapment of inclusion particles.

As an example, Figure 15[27,28] simulates what happens to 15,000 inclusion particles that are suddenly added into the flow through the nozzle ports. These particles actually represent plastic beads in the water model, with a density of 988 kg/m^3, chosen to approximate the flotation velocity of 300 μm alumina inclusions in steel.[29] Note how the particles travel with the jet to the narrow face (1.6 seconds). At the same time, they gradually float upward (2.6 seconds). After impinging on the narrow face, they split into two groups (10 seconds), which move into the upper and lower recirculation zones. Within 2 minutes, they are well mixed with the liquid.

Examples of the paths taken by individual particles are shown in Figure 16.[27] Some particles (upper-left side) circulate in the upper roll and touch the top surface, where they are likely removed. Other particles circulate in the upper zone (lower-left side), the short-circuit flow region (upper-right side), or the lower zone (lower-right side), but eventually end up deep in the caster, where they likely are trapped to form internal defects.

Note the thin black line at the upper-left side of Figure 15, which represents where a screen was inserted in the water model to capture inclusions in a crude approximation of removal into the slag layer.[29] Particles in the upper recirculation zone that cross the screen line are computationally trapped as well. The predicted and measured entrapment fractions after 10 seconds are 22 and 27 pct, and then, after 100 seconds, are 53 and 50 pct, respectively. If accurate

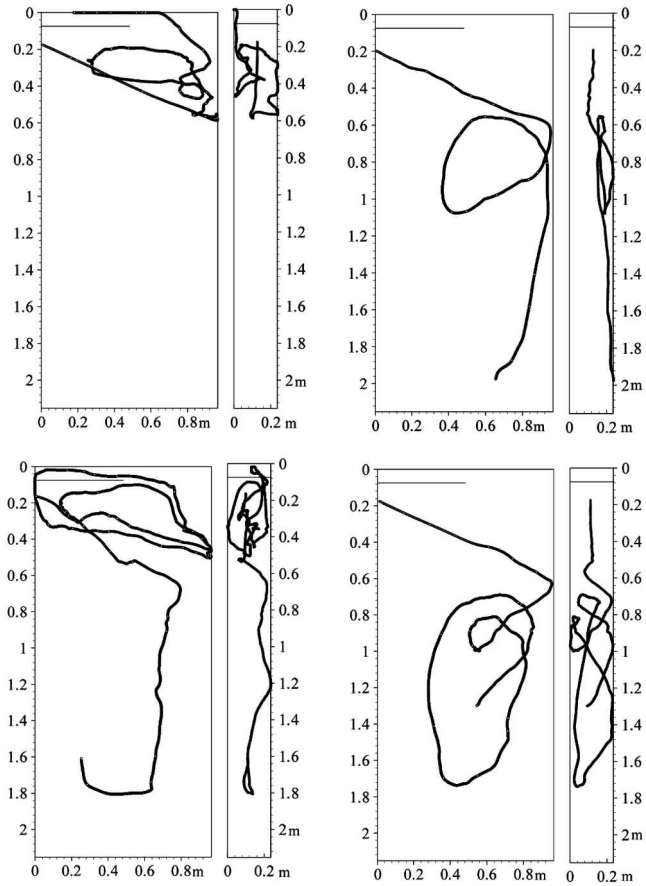

Fig. 16—Four typical particle trajectories predicted by the computation.

entrapment criteria and drag coefficients can be found for different types of inclusions, this modeling tool could be applied to optimize inclusion removal in the design of mold flow patterns.

B. *Shell Solidification: Thin-Slab Caster*

To build on the accuracy of the early solidification models in the mold, the delivery of superheat from the impinging jet onto the solidification front should be taken into account. This effect might explain the slight discrepancy between the model and measurements in Figure 1. At high superheats and casting speeds, this is also a practical concern, particularly on the narrow face just below the mold, where breakouts may occur if the shell becomes locally thin. Quantifying these effects is a task ideally suited to computational models, with the aid of careful measurements.

As an example to test the current models, 3-D fluid flow and heat transfer was modeled in the molten steel, interface, and mold[30] and compared with extensive experimental measurements conducted on the AK Steel–Mansfield stainless steel caster.[31] The test casting conditions include a 132 mm mold thickness, 965 to 984 mm mold width, 127 mm nozzle submergence depth (meniscus to top of port), 25.4 mm/s casting speed, and 57 °C to 61 °C superheat for 434 stainless steel with a 1502 °C liquidus temperature.

The first step in modeling shell growth is to obtain an accurate flow field. Three-dimensional turbulent flow of molten steel through the nozzle into the mold cavity was modeled with the finite-difference code CFX 4.2,[32] using the standard K-ε turbulence model and a fixed, structured grid.[30] The computational domain includes both the nozzle and mold.[33] The predicted velocity vectors are superimposed on a photograph of a water model of the process in Figure 17.[30] The agreement seems reasonable: the flow pattern is a typical double roll with an extra jet issuing down from a small hole in the nozzle bottom. This is presumably done to help stabilize the flow pattern against transient oscillations from side to side. Note that this central jet is not perfectly symmetrical, although the model assumes that it is.

Next, the corresponding steady heat-conduction equation was solved to predict the distribution of the superheat in the liquid pool. The calculated temperature distribution is shown in Figure 18. Heat is seen to follow the flow as the liquid cools. The narrow-face meniscus has the coolest liquid. To validate the predictions, temperatures in the molten steel were measured by inserting a thermocouple probe downward through the top surface into the molten steel at several locations and depths in the operating thin-slab caster. The temperature profiles are compared in Figure 19[30] with increasing depth beneath the surface. The steel/slag-layer interface is identified by the sharp change in measured temperature. The meniscus itself retains about 30 pct of the total superheat temperature difference. Beneath the surface, the measurements fluctuate a little, likely due to turbulent flow transients. The model predicts a slight fall, but still appears to agree reasonably.

Next, solidification of the steel shell was simulated using CON1D,[34] a simple 1-D transient solidification model of the shell, coupled together with a 2-D analytical solution of steady temperature in the mold. The heat flux calculated from the fluid-flow model, shown in Figure 20,[30] is incorporated as the boundary condition on the solidification front. The large peak is where the jet impinges on the narrow face. It even exceeds heat extraction to the mold at this point. The wide face has just a tiny increase where the small central jet touches it, which is small relative to the mold heat extraction.

Heat transfer through the shell and mold is governed mainly by the size and properties of the interfacial gap. Thus, the CON1D model features mass and momentum balances on the flux layers in the gap, thermal resistance from the surface roughness of the shell, radiation conduction, and other important phenomena.[34] Because many of these gap properties are not known, the model was calibrated using temperature measurements from thermocouples in the copper mold.[31] To account for the complexities of the water slot and mold geometry near the thermocouple, these temperatures were first interpreted using a full 3-D finite-element model of portions of the copper mold plate, as shown in Figure 21.[30] The 3-D model results were then analyzed to determine "offset" factors to calibrate the simple CON1D model to almost exactly match both the 3-D model predictions and the measurements. The calibrated heat-flux curves are also included in Figure 20.[30] The extent of this calibration is shown by the agreement between the predicted and measured temperatures in Figure 22.[30] For true validation of the model, its predictions were compared with the total heat extraction based on the cooling-water temperature difference. They matched within about 10 pct.

Having calibrated the model, it was run under the transient

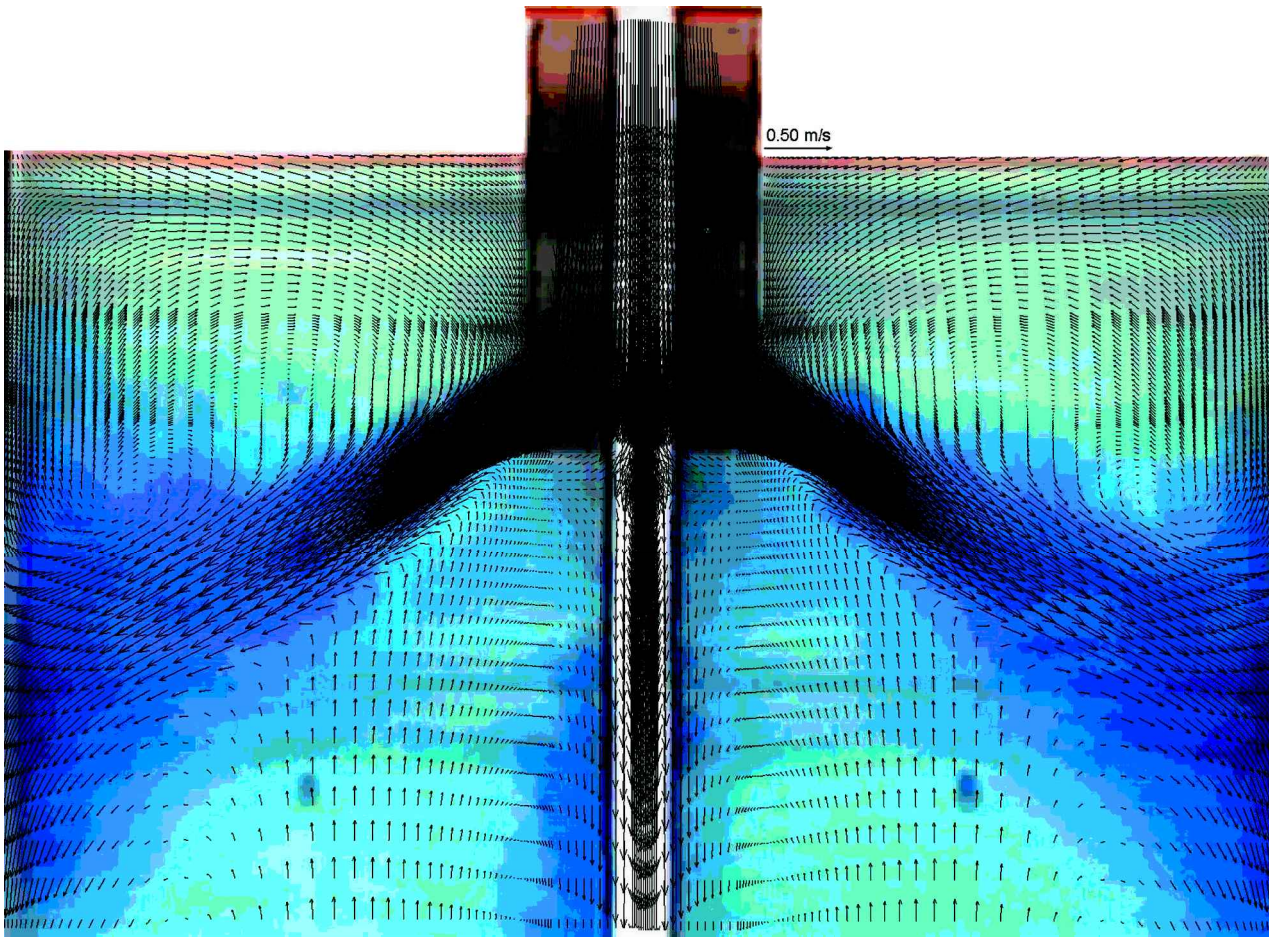

Fig. 17—Calculated velocity vectors superimposed on the water model during die injection.

conditions present during a breakout. The predicted shell-thickness profiles are compared in Figure 23[30] down the wide face and in Figure 24[30] down the narrow face, with many shell-thickness profiles measured from the breakout shell. The agreement is significant because there are no adjustable parameters left in the model. Note the expected thinning of the shell near the narrow face where the steel jet impinges, which is different between the steady-state and transient conditions of the breakout.

This work demonstrates the quantitative ability of this modeling approach to simulate coupled fluid flow and solidification heat transfer in a real steel continuous casting process. This particular example is also of practical interest, because the shell thinning was acceptable, in spite of the high superheat. This is because the shell remained in reasonable contact with the mold. Other studies[35] have shown that if the gap resistance is too high, such as from inadequate taper, then shell thinning due to jet impingement is much more severe and will cause breakouts. As a further model application, simulations could explore the effect of increasing casting speed, knowing the minimum shell thickness needed to prevent cracks and breakouts below the mold, from separate model studies.[36]

C. *Shell Solidification: Billet Caster Corners*

Another practical example of shell-thickness prediction is the corner of a billet section during solidification in the mold. This is important, because longitudinal corner cracks will result when cooling of the corners in the mold is either excessive or insufficient. For the latter case, thin corners are caused when an insufficient taper allows the corner region to pull away from the mold wall. This forms a gap with high thermal resistance that decreases heat conduction across the interface.

To model this phenomenon requires coupling a 2-D transient heat-transfer model with a stress model to predict both the temperature and shrinkage of the shell. Iteration is needed between the models because the temperature controls the shrinkage, but the shrinkage also affects the temperature development. As before, the heat transfer across regions of good contact was calibrated using mold thermocouples and validated with heat extraction by the mold cooling water and with shell-thickness measurements. Across the gap, whenever and wherever it forms, heat transfer is controlled by conduction and radiation through a hydrogen-air mixture. In addition to the thermal strains, the stress model includes time- and temperature-dependent viscoplastic functions to model the creep and plastic strains.

An example from such a model of the temperature and shape predictions in the corner region of a typical 120-mm-square billet of 0.04 pct C steel solidifying in the mold is shown in Figure 25,[37] cast at 2.2 m/min with only a 0.78 pct/m taper. The shrinkage exceeds the taper for this case, so the shell pulls away from the mold corner within 1 second

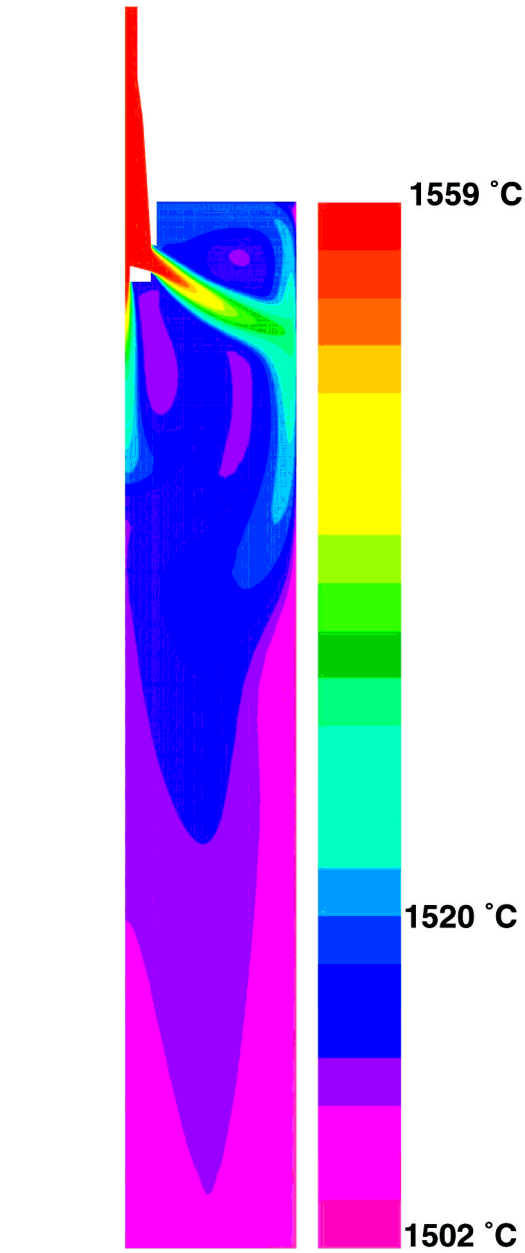

Fig. 18—Temperature contours calculated in the molten steel pool.

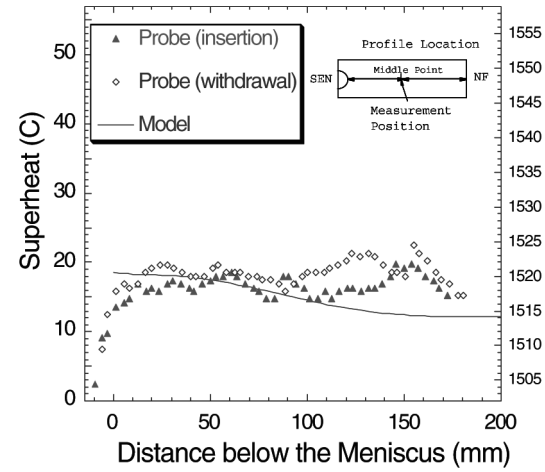

Fig. 19—Temperature in molten steel (measurements compared with calculations).

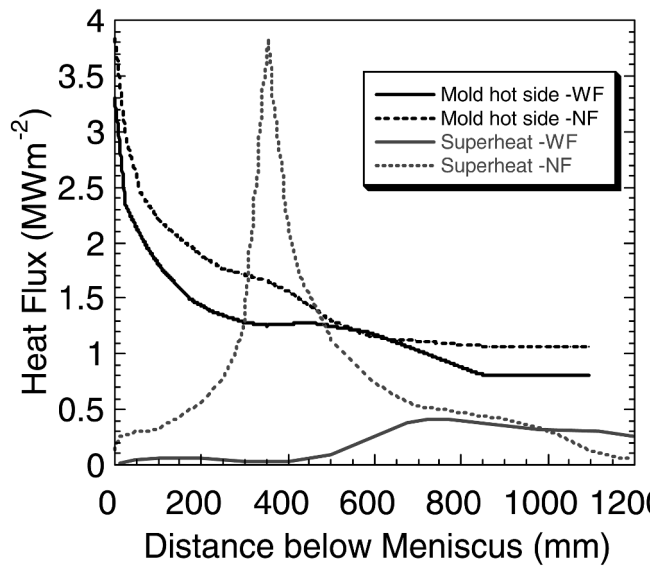

Fig. 20—Liquid/shell and shell/mold heat flux profiles down the strand centerlines.

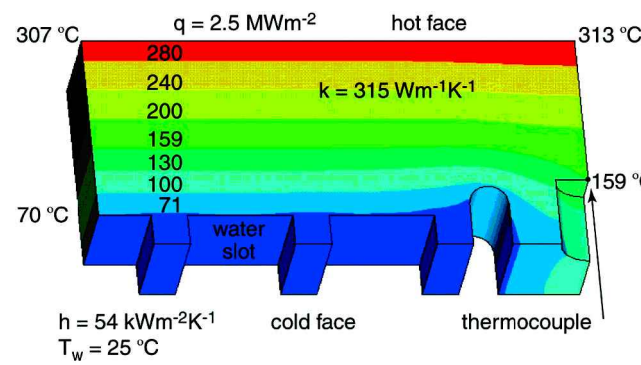

Fig. 21—Temperature contours in 3-D portion of mold wall showing thermocouple position and temperature.

below the meniscus. The gap quickly slows down heat transfer. This makes the corner of the shell hotter and thinner than the rest of the shell, which is kept in good contact with the mold walls due to the ferrostatic pressure.

The entire billet cross section is shown in Figure 27,[37] with the calculations on the right-hand side compared with a sulfur print of an actual billet section (285 mm below the meniscus) on the left-hand side. The solid shell front was revealed at a known instant by adding an FeS tracer to the mold during casting. The predicted and measured shell thinning around the corner is about the same, so the model appears to be valid.

This typical mold had a rounded corner with a 4 mm radius, which produced a fairly short gap region. Figure 26[37] shows the consequence of increasing the corner radius to 15 mm with everything else staying the same. The gap is seen to grow wider and to extend farther around the perimeter. This is because the larger corner radius causes behavior closer to that of a round section, which tends to form a gap that extends around the entire perimeter. The

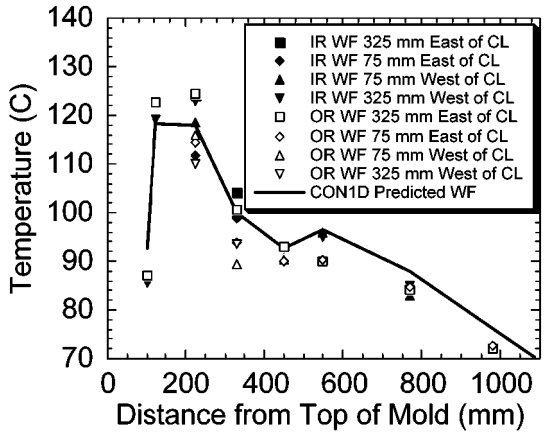

Fig. 22—Temperatures down the wide face mold wall (calculated and measured).

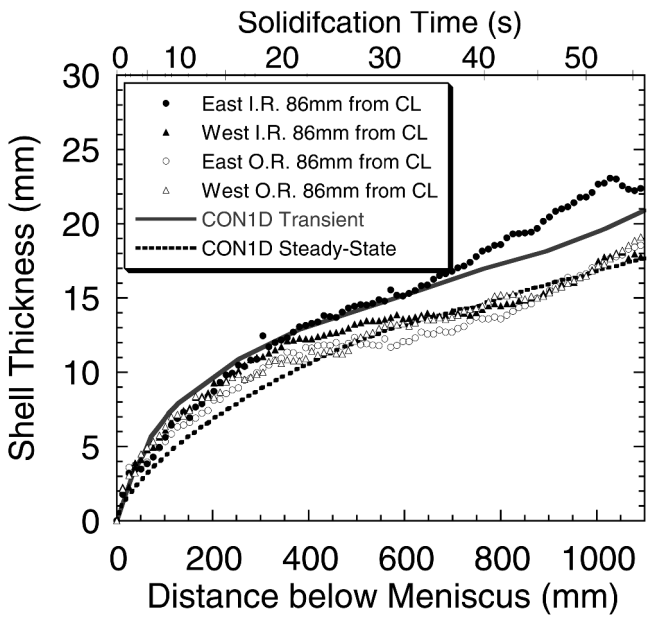

Fig. 23—Shell thickness along the wide face (calculated compared with the breakout shell measurements).

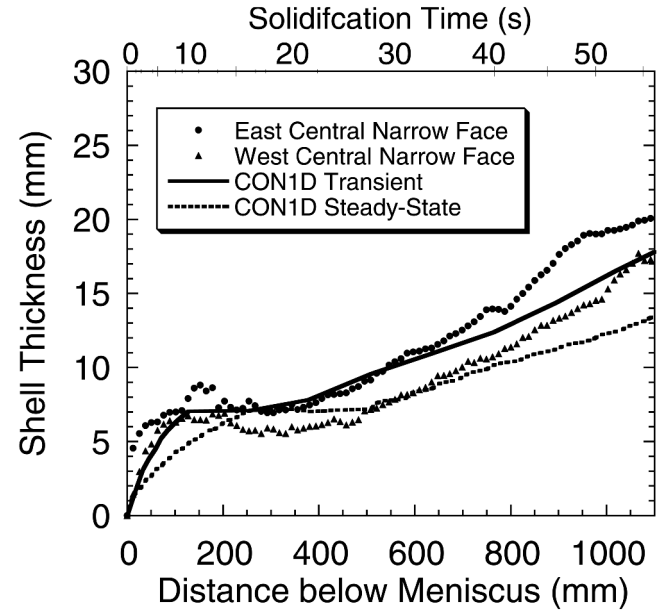

Fig. 24—Shell thickness along the narrow face (calculated compared with the breakout shell measurements).

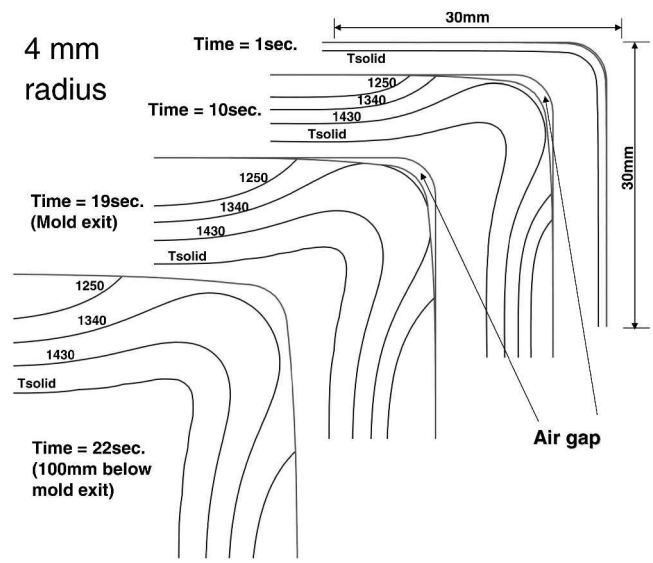

Fig. 25—Shell growth calculated in the corner region of a 120-mm square billet with 4-mm corner radius.

result is a greater reduction in heat transfer in the corner region and, consequently, a hotter and thinner shell. This shell is, thus, locally weaker and subjected to more stretching. Thus, it is more prone to longitudinal corner cracks. This is confirmed in both the stress-analysis results and in plant experience.

If heat flux could be made more uniform, such as by optimizing the taper or using mold flux, then sections with larger-radius corners might be castable without cracks. Similarly, billets with more-uniform cooling around the perimeter should be able to withstand higher casting speeds without forming off-corner subsurface cracks due to excessive bulging below the mold. More research is planned to investigate this.

D. *Mold Thermal-Fatigue Analysis*

Building on the early work of Brimacombe (with Samarasekera and Anderson),[38] 3-D finite-element models of thermal distortion can now be extended to predict crack formation, including creep and plastic strain accumulated over many fatigue cycles.[39,40,41] An important application is the study of surface cracks in the copper plates near the meniscus of thin-slab casting molds.

For example, Figure 28[41] shows short longitudinal cracks on the surface of a thin-slab funnel mold, which formed beneath cracks in the protective Cr coating layer. This exposed the copper to Zn residuals in the steel that penetrated to form brass. Such cracks are a major concern because they directly cause longitudinal cracks in the steel shell, reduce mold life, and even pose a potential safety threat if they propagate too deep.

Figure 29[41] shows the temperature and distorted shape

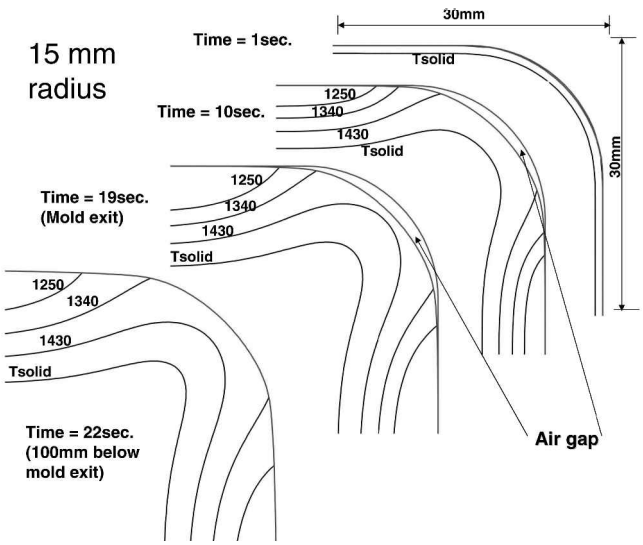

Fig. 26—Shell growth in a mold with 15-mm radius, showing increased gap size, shell temperature, and shell thinning in the corner.

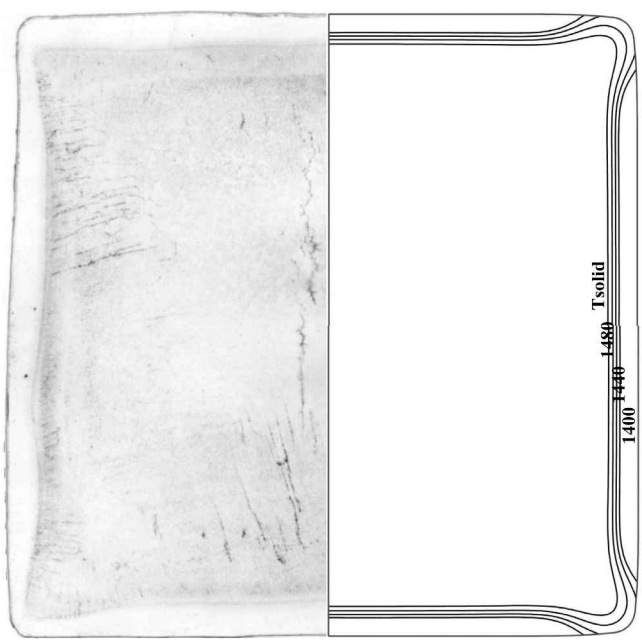

Fig. 27—Calculated temperatures in the transverse billet section compared with the measured shell shape.

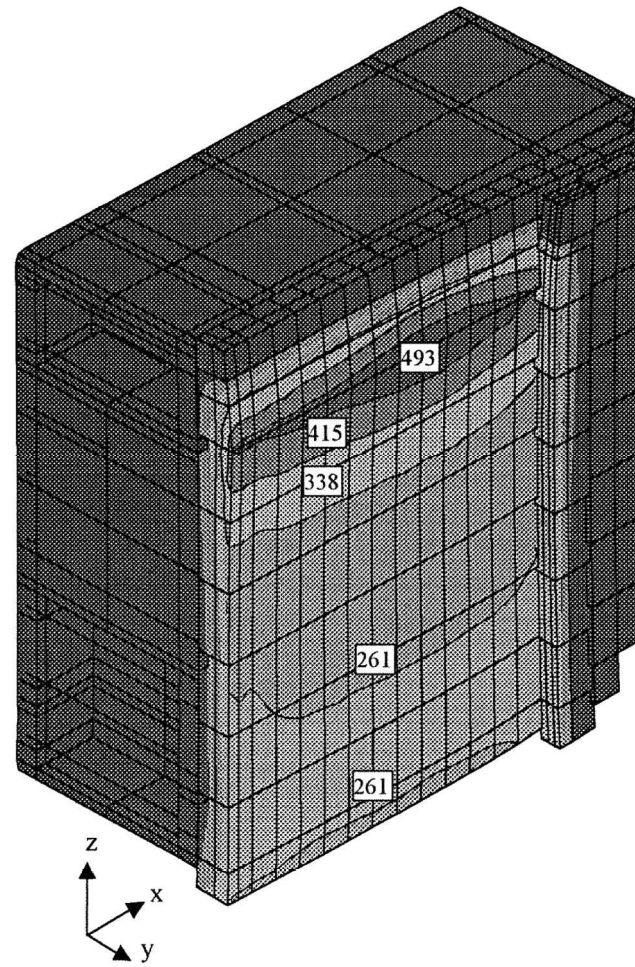

Fig. 29—Calculated temperatures and distorted shape of the thin slab mold.

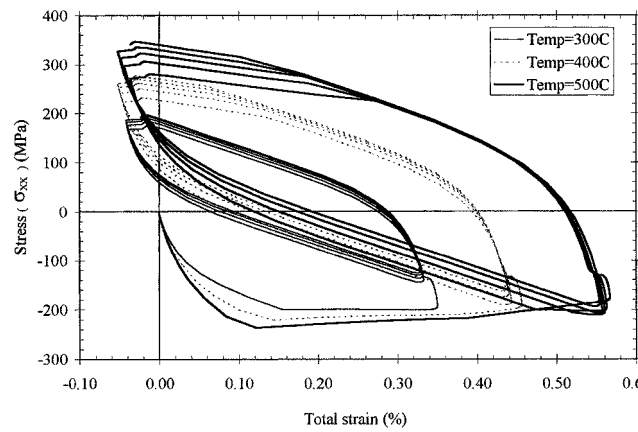

Fig. 30—Calculated stress-strain histories at the point of crack location in a funnel mold.

of a thin-slab mold during operation, from a finite-element simulation developed to investigate this problem. To accurately model the thermal distortion, it is important to include the backing plate and water box, which adds rigidity to lessen the bending of the copper plates. To accurately predict the temperatures, the hotface heat flux was calibrated with thermocouple measurements inside the mold walls.[42] The resulting temperature contours, also included in Figure 29, quantify the extent of a hot spot just below the meniscus, which is greater in the off-corner region of a funnel mold.[41]

Next, the model calculates stress and strain histories, based on the alternating between room temperature and steady-state temperature profile during operation, including time- and temperature-dependent elastic-viscoplastic constitutive equations. Figure 30[41] shows examples of the stress-strain hysteresis loops experienced across the crack location for three different maximum temperatures. Each loop corresponds to the thermal cycle of one casting sequence: five sequences are shown at each temperature. Upon heating, the surface expands and goes into compression, owing to constraint by the colder copper beneath. Without inelastic

strain, the stress would have returned to zero after cooling. However, the stress at high temperature generates compressive inelastic strain. This causes the stress to overshoot into tension after cooling. The tension generated by each heating and cooling cycle causes fatigue damage to accumulate with each cycle. At higher temperatures, both the stress and strain amplitudes are greater.

In addition to the large cycles caused each time the mold is filled at ladle exchanges, many smaller fatigue cycles occur due to level fluctuations (not shown here). Other model calculations show that the low-frequency (0.05 Hz) liquid-level fluctuations measured in the funnel mold lead to greater thermal transients, which increase the amplitude of the fatigue cycles. The high-frequency level fluctuations (0.3 Hz) observed in the parallel mold are predicted to produce less fatigue damage. The inelastic strain accumulated from different types of fatigue cycles is added together using Minor's law. Based on experimental fatigue data, the number of cycles to failure can be predicted, which roughly matched the lifetimes observed in the plant.

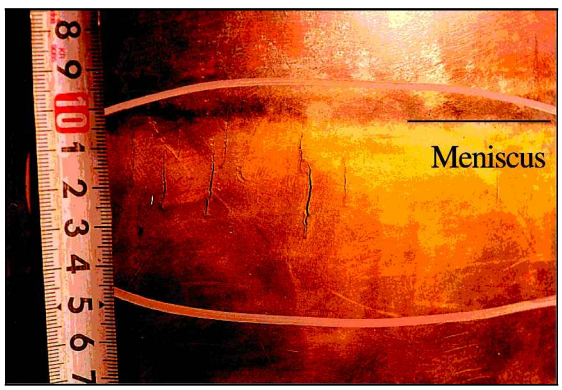

Fig. 28—Longitudinal cracks on the hot face near the meniscus of the thin slab mold.

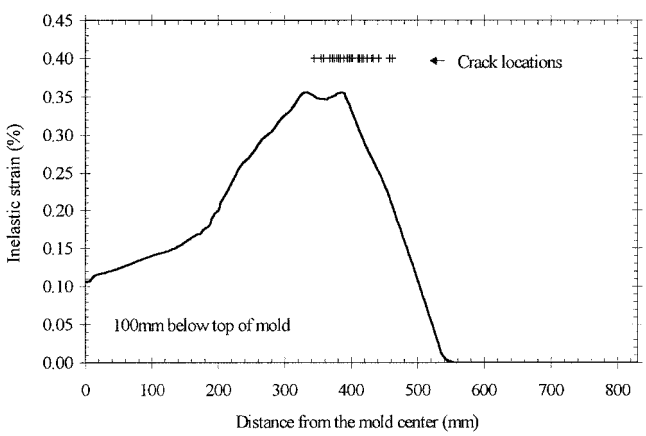

Fig. 31—Inelastic strain profile across the mold perimeter at 100 mm below the top of the mold.

Figure 31[41] shows the inelastic strain profile (which is the plastic and creep strain added together) calculated across the mold width near the meniscus where the cracks were observed. Both the inelastic strain and the accompanying transverse stress were greatest at the off-corner location, where the temperature was highest. This region was hottest, owing in part to the local water-slot design in that region of the funnel. Most significantly, this location is also where the cracks formed on the mold surface.

Thus, the model shows that the detrimental fatigue strains which caused the cracks in the funnel mold were due to the high-temperature cycling at that location. The results suggest that cracking might be avoided by changing the slot design to decrease the maximum surface temperature, by loosening clamping to lower the mold constraint, and by decreasing the extent of low-frequency level fluctuations.

E. *Modeling Bulging and Internal Cracks*

Following the success of Brimacombe in applying models to understand cracks generated from thermal stress, many stress models were developed in the 1980s to predict mechanical strains due to bulging below the mold. Some estimated bulging with analytical solutions from beam bending.[43–46] Early finite-element models were developed by Schwerdtfeger,[47,48] by Rammerstorfer,[49] and, later, by several others.[50–54]

As computer advances enable better simulations, more bulging and unbending studies are being performed today.[55,56,57] For example, Figure 32[56] shows finite-element computations of inelastic strain in a longitudinal section through the strand shell, while it moves downstream over a uniform sequence of rolls. The contours are superimposed on the magnified distortions, to show the well-known

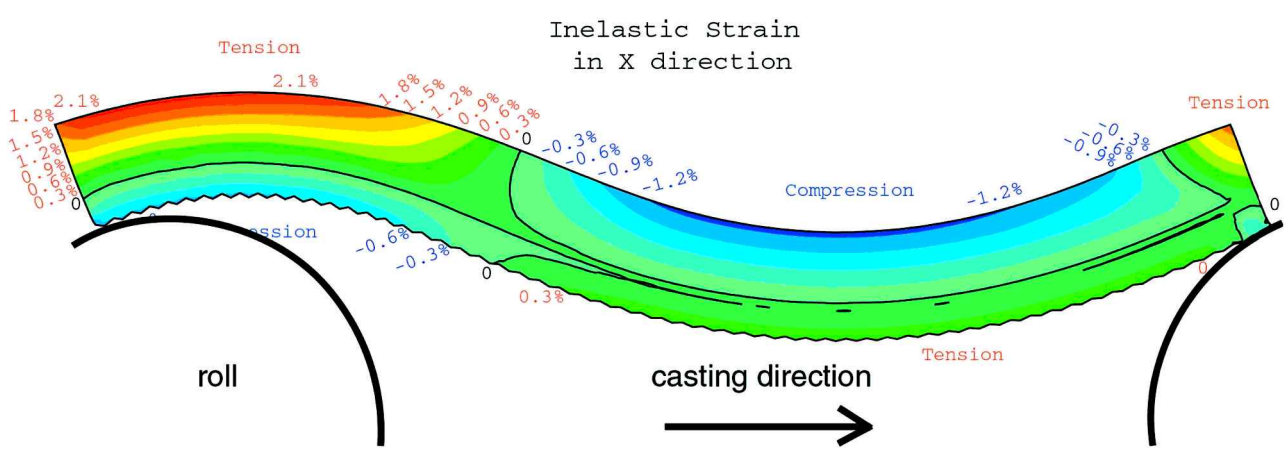

Fig. 32—Inelastic strain contours and distorted shapes of the strand section between rolls (magnified).

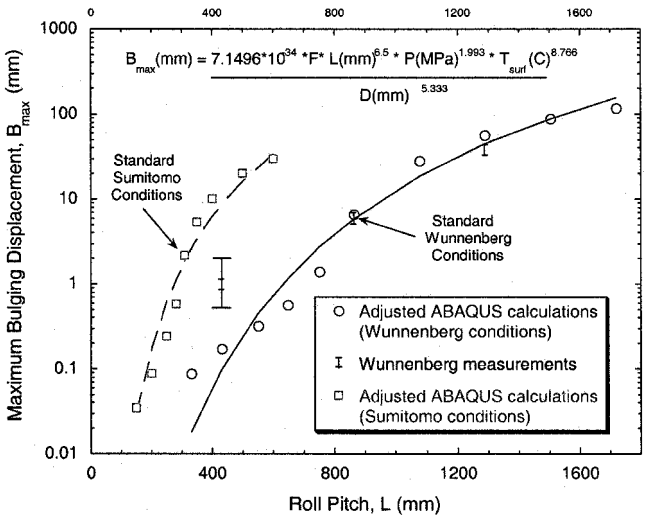

Fig. 33—Roll pitch effect on the maximum bulging displacement comparing calculation and measurements.

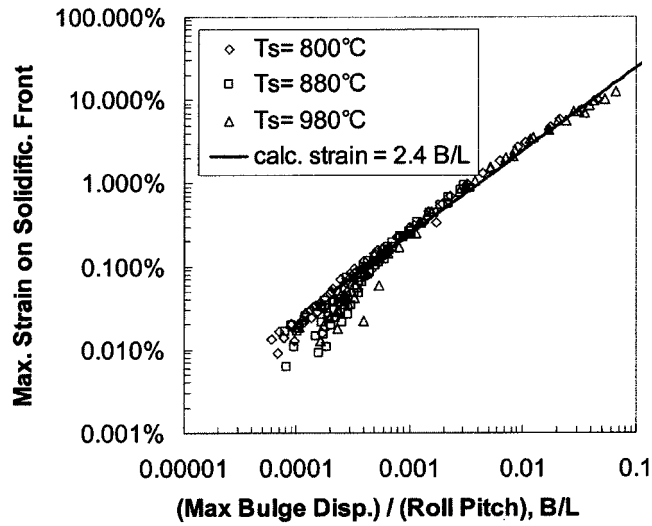

Fig. 34—Correlation between the maximum bulge displacement and strain on the solidification front.

phenomena[53,58,59] of "negative bulging" just past the upstream roll and the downstream movement of the point of maximum bulge past the midway point between rolls. These effects are due to the upward deflection of the strand when it first contacts the upstream side of the roll, like a water skier bouncing over gentle waves. This is modeled by imposing boundary conditions that force the shell shape on the left- and right-hand sides of the roll pitch to match, which is reasonable for a pseudosteady state. Note that the most detrimental strains are in the tensile regions found across the solidification front almost directly above the rolls.

Although measurements of bulging during operation are difficult, they are critical for model validation. Two such measurements were performed by Wunnenberg and Huchingen[60] and on a Sumitomo pilot caster.[58,61] The conditions of Wunnenberg and Huchingen are simulated in Figure 32, (cast at 0.85 m/min, with a 1350 mm width, 860 mm pitch, 0.27 MPa pressure, 79 mm shell thickness, and 1000 °C average surface temperature). With less severe bulging, the effects of strand movement (negative bulging, *etc.*) are often negligible, and a simpler static analysis yields similar results.[57]

Having a validated model, extensive parametric studies can be performed to reveal the important trends. Many such past studies have quantified that the most important factors causing bulging are a larger roll pitch, hotter surface temperature, thinner shell, and higher ferrostatic pressure. Increasing the casting speed is indirectly detrimental, because it causes a hotter, thinner, and weaker shell. For example, Figure 33[56] shows the effect of roll pitch on maximum bulging displacement, compared with a few measurements. The log scale of this graph clearly shows the tremendous benefit of shortening the roll pitch in half to reduce bulging by 30 times. The results of many computations can be curve-fit to produce an empirical equation to predict bulging, which is also shown. Similar models have been applied to generate similar empirical equations by several previous modelers[45,54] and are widely used in caster design.

Such model-generated knowledge has naturally led to lowering the roll pitch as much as possible. In slab casting, the limitation of the roll diameter itself has been surmounted with split rolls. This allows smaller diameter, and closer-spaced, rolls, which can still safely support the steel-strand loading with minimal bending, owing to their shorter length.

The bulging-model results can be used further to produce relations to predict strain across the solidification front. The results from 70 such finite-element computations are presented in Figure 34,[57] which shows that this detrimental bulging strain can be predicted surprisingly well with a simple linear equation. The maximum strain on the solidification front equals about 2.4 times the ratio of the maximum bulging displacement to the roll pitch.

Applying the results to prevent cracking has been met with more difficulty, because crack formation is so difficult to model and is not completely understood. Thus, to design casters that avoid internal cracks, models are currently used only qualitatively or by extensive calibration with plant measurements. Careful lab experiments applying load to a solidifying steel shell have quantified that strains of about 1 to 2 pct are needed to cause cracks.[62,63,64] It remains a mystery that model-predicted inelastic strains in a modern slab caster are roughly 10 times smaller than this, and yet cracks still may occur.[19] Some suggest that the damage accumulates over successive roll pitches.[63] Other possible explanations are considered next.

One important phenomenon is the transient nature of bulging. Gancaerz and co-workers pointed out in 1991 that bulging over a series of rolls is different than over a single roll pitch.[53,56] This is because inevitable disturbances, such as those caused by casting-speed transients, changes in roll pitch between segments, or misalignment, propagate a long way downstream before steady state is reached again. Our recent work has confirmed that at the transition between two segments with different roll pitches, the bulging is greater than at steady state in either segment.[53,56] A second phenomenon is roll misalignment, due to maintenance-tolerance variations, roll wear, thermal distortion, and other causes. Figure 35[56] illustrates some of the features of both of these, as it presents simulations of a long section of strand passing over a sequence of eight rolls, where the second roll is misaligned.

This figure shows that the strand generally bulges exactly

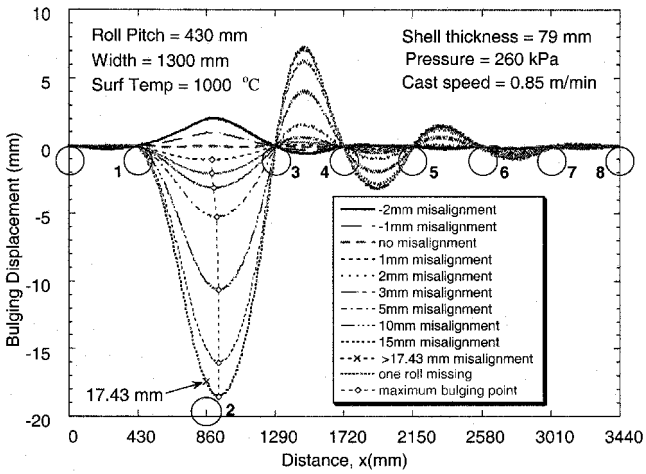

Fig. 35—Effect of the roll misalignment on bulging between rolls for a steel shell that spans eight roll pitches.

as much as the roll is misaligned. The disturbance is then propagated several rolls downstream, alternating between negative bulging and excessive positive bulging. Such disturbances can be recognized from roll-force sensor measurements, if they record alternating high and low forces on successive downstream rolls.

The bulging is less than the misalignment only if the strand can support itself across twice the roll pitch. This is unlikely except in cases of severe misalignment. Increasing the water spray cools and strengthens the strand surface, which would help to reduce bulging strain only for those severe misalignment cases. A much better solution is to pay careful attention to the submold roll support and roll alignment. This is crucial to avoiding internal cracks when casting crack-sensitive grades at high speed or with large section sizes that are prone to bulging.

VI. THE FUTURE

To implement results into the plant, simply publishing the modeling study is not enough. As Brimacombe often lamented, "the best way to hide important findings is to publish them in the open literature." To help achieve technology transfer, he traveled the world to teach short courses to plant operators and developed an expert system, CRACK-X, which could diagnose cracking problems in a billet caster. The best way to implement modeling results, however, is to let the model itself control the process by running online. Brimacombe envisioned an "intelligent mold" controlled by an advanced process model.[65] Such a model would simultaneously manage the flow control, casting speed, narrow-face taper, mold and spray cooling water, powder feeding, and electromagnetic forces in order to minimize defects. By responding to sensor feedback, including the liquid level, thermocouple signals, mold friction, and, perhaps, even molten-steel velocity sensors, such a model could also identify impending problems and take immediate corrective action.

The use of online control models has already started. Spray water flow rates are now routinely controlled dynamically using 1-D finite-difference models[66,67] as open-loop control models that update at least every minute. While similar models taxed the fastest computers when applied by Brimacombe in 1974, today's optimized versions can execute in a split second to quantify heat transfer throughout the caster. These models adjust water flow to ensure that each portion of the strand surface experiences the desired thermal history. This is especially important, and not always intuitive, during and after transients such as casting slowdowns during ladle exchanges.

Breakout detection systems were the first practical example of the intelligent mold and are in widespread use in slab casters. This was made possible by the discovery of the thermal "signature" of a sticker breakout.[68] Some companies now output online thermal maps, which show the operator evolving color contour plots of mold temperature, constructed from the signals from many thermocouples.[69] Once the thermal signatures of other defects are clearly understood, online models could be developed to take appropriate action. Thus, more and better online models are expected in the future.

Offline models are still needed to improve process understanding. Faster computers will enable existing models to perform large parametric studies for true optimization, rather than to simply demonstrate their capability, as is often done today. There should be more comprehensive studies with the advanced models, followed by reduction to simple empirical equations that can be applied in process design. The same modeling effort that has gone into bulging for roll-system design should be applied to other areas. For example, taper design and casting speed should be optimized to minimize mold gaps, in order to avoid bulging below the mold, for unsupported billets, or narrow-face breakouts due to shell thinning, for high superheats.

Future models will need to combine even more phenomena together. For example, adding deformation to the solidification models would help one to understand and improve thin-slab and strip casters. Prediction of internal cracks, for example, will eventually benefit from microstructural prediction and thermodynamic models which track the formation of harmful embrittling precipitates together with temperature and the tensile stresses that cause cracks. Controlled laboratory experiments of mechanical properties, precipitation, and microstructure are needed to develop the fundamental knowledge base for these models. Finally, more transient simulations are needed, following more of the process steps. With tools evolving to achieve these goals, the future potential for modeling has never looked better.

VII. CONCLUSIONS

Early modeling pioneers, including Keith Brimacombe, showed us how to develop mathematical models, validate them with experiments and plant trials, and apply them to gain insight and solve practical problems in processes such as the continuous casting of steel. Great advances in computer power now enable models to tackle a wide range of phenomena with more realism and accuracy than ever. However, Brimacombe also taught that future advances to the continuous casting process will not come from either models, experiments, or plant trials. They will come from ideas generated by people who understand the process and the problems. This understanding is rooted in knowledge, which can be confirmed, deepened, and quantified by tools that include computational models. As our computational tools continue

to improve, they should grow in importance in fulfilling this important role, leading to future process advances.

ACKNOWLEDGMENTS

I thank the sponsoring steel companies in the Continuous Casting Consortium, University of Illinois, for funding and experimental data that has made our research possible, the National Science Foundation (Grant Nos. DMI-9800274 and 0115486) for funding, and the National Center for Supercomputing Applications, the University of Illinois, for computing time. I also thank the many students and visitors in my group who produced the research results presented here, including Hua Bai, David Creech, Tiebiao Shi, Ya Meng, Quan Yuan, Sivaraj Sivaramakrishnan, Joon-kil Park, Lan Yu, and Kuan-Ju Lin. Finally, I am grateful to have had the privilege to learn from such a great man as Keith Brimacombe, who was and still is an inspiration.

REFERENCES

1. I.V. Samarasekera: *Metall. Mater. Trans. B*, 2002, vol. 33B, pp. 5-29.
2. A.W.D. Hills: *J. Iron Steel Inst.*, 1965, vol. 203, p. 18.
3. N. Chvorinov: *Giesserei*, 1940, vol. 27, pp. 201-08.
4. J. Savage and W.H. Pritchard: *Iron Steel Inst.*, 1954, vol. 178, pp. 269-77.
5. I.V. Samarasekera and J.K. Brimacombe: in *Mold QI1 eration for Quality and Productivity*, A.W. Cramb and E.S. Szekeres, eds., ISS, Warrendale, PA, 1991, pp. 55-67.
6. E.A. Mizikar: *Trans. TMS-AIME*, 1967, vol. 239, pp. 1747-53.
7. J. Lait, J.K. Brimacombe, and F. Weinberg: *Steelmaking*, 1974, vol. 2, pp. 90-98.
8. J.E. Lait, J.K. Brimacombe, F. Weinberg, and F.C. Muttitt: *Open Hearth Conf. Proc.*, ISS, Warrendale, PA, 1973, vol. 56, pp. 269-302.
9. J. Szekely and R.T. Yadoya: *Metall. Mater. Trans.*, 1973, vol. 4, pp. 1379-88.
10. J. Szekely and V. Stanek: *Metall. Trans.*, 1970, vol. 1, pp. 119-26.
11. J. Szekely and S.T. DiNovo: *Metall. Trans. A*, 1974, vol. 5, pp. 747-54.
12. J.K. Brimacombe: *Can. Metall. Q.*, 1976, vol. 15 (2), pp. 163-75.
13. R.B. Mahapatra, J.K. Brimacombe, and I.V. Samarasekera: *Metall. Trans. B*, 1991, vol. 22B, pp. 875-88.
14. S. Kumar, J.A. Meech, I.V. Samarasekera, and J.K. Brimacombe: *Iron Steelmaker*, 1993, vol. 20 (9), pp. 29-36.
15. B.G. Thomas and B. Ho: *J. Eng. Industry*, 1996, vol. 118 (1), pp. 37-44.
16. I.V. Samarasekera and J.K. Brimacombe: *Ironmaking and Steelmaking*, 1982, vol. 9 (1), pp. 1-15.
17. R. Dippenaar, I.V. Samarasekera, and J.K. Brimacombe: *Ironmaker Steelmaker (ISS Trans.)*, 1986, vol. 7, pp. 331-43.
18. A. Grill, J.K. Brimacombe, and F. Weinberg: *Ironmaking and Steelmaking*, 1976, vol. 3 (1), pp. 38-47.
19. K. Sorimachi and J.K. Brimacombe: *Ironmaking and Steelmaking*, 1977, vol. 4, pp. 240-45.
20. K. Kinoshita, T. Emi, and M. Kasai: *Tetsu-to-Hagané*, 1979, vol. 65 (14), pp. 2022-31.
21. J.O. Kristiansson: *J. Thermal Stresses*, 1982, vol. 5, pp. 315-30.
22. J.E. Kelly, K.P. Michalek, T.G. O'Connor, B.G. Thomas, and J.A. Dantzig: *Metall. Trans. A*, 1988, vol. 19A, pp. 2589-2602.
23. V.R. Voller and F. Porte-Agel: *J. Computational Phys.*, 2002, vol. 179, pp. 1-6.
24. B.G. Thomas and L. Zhang: *Iron Steel Inst. Jpn. Int.*, 2001, vol. 41 (10), pp. 1185-97.
25. S. Sivaramakrishnan, H. Bai, B.G. Thomas, P. Vanka, P. Dauby, and M. Assar: *Ironmaking Conf. Proc.*, Pittsburgh, PA, ISS, Warrendale, PA, (Pittsburgh, PA, March 26–29, 2000), 2000, vol. 59, pp. 541-57.
26. B.G. Thomas, Q. Yuan, S. Sivaramakrishnan, T. Shi, S.P. Vanka, and M.B. Assar: *Iron Steel Inst. Jpn. Int.*, 2001, vol. 41 (10), pp. 1266-76.
27. Q. Yuan, S.P. Vanka, and B.G. Thomas: *2nd Int. Symp. on Turbulent and Shear Flow Phenomena*, (Stockholm, Sweden, June 27–29, 2001), Royal Institute of Technology (KTH), Stockholm, 2001, vol. 2, pp. 519-24.
28. B.G. Thomas, Q. Yuan, S. Sivaramakrishnan, and S.P. Vanka: *J. Met.*: JOM-e, http://www.tms.org/pubs/journals/JOM/0201/Thomas/Thomas-0201.html, 2002.
29. R.C. Sussman, M. Burns, X. Huang, and B.G. Thomas: *10th Process Technology Conf. Proc.*, Toronto, Canada, Apr. 5–8, 1992, ISS, Warrendale, PA, 1992 vol. 10, pp. 291-304.
30. B.G. Thomas, R. O'Malley, T. Shi, Y. Meng, D. Creech, D. Stone: *Modeling of Casting, Welding, and Advanced Solidification Processes*, Aachen, Germany, Aug. 20–25 2000, Shaker Verlag GmbH, Aachen, Germany, 2000, pp. 769-76.
31. B.G. Thomas, R.J. O'Malley, and D.T. Stone: *Modeling of Casting, Welding, and Advanced Solidification Processes*, San Diego, CA, TMS, Warrendale, PA, 1998, vol. VIII, pp. 1185-99.
32. Report CFX 4.2, AEA Technology, Pittsburgh, PA, 1998.
33. D. Creech: Masters Thesis, University of Illinois at Urbana–Champaign, Urbana, IL, 1998.
34. B.G. Thomas, B. Ho, and G. Li: in *Alex McLean Symp. Proc., Toronto*, (Toronto, Canada, July 12–14, 1998), ISS, Warrendale, PA, 1998, pp. 177-93.
35. G.D. Lawson, S.C. Sander, W.H. Emling, A. Moitra, and B.G. Thomas: in *Steelmaking Conf. Proc.*, ISS, Warrendale, PA, Chicago, IL, 1994, vol. 77, pp. 329-36.
36. C. Li and B.G. Thomas: *Brimacombe Memorial Symp.*, Vancouver, Canada, Canadian Institute of Mining and Metallurgy, Montreal, 2000, pp. 595-611.
37. J.-K. Park, B.G. Thomas, Y. Meng, and I.V. Samarasekera: "Analysis of Thermo-Mechanical Behavior in Billet Casting," Report, University of British Columbia, Vancouver, 2001.
38. I.V. Samarasekera, D.L. Anderson, and J.K. Brimacombe: *Metall. Trans. B*, 1982, vol. 13B, pp. 91-104.
39. T. O'Conner and J. Dantzig: *Metall. Mater. Trans. B*, 1994, vol. 25B, pp. 443-57.
40. G. Li, B.G. Thomas, and J. Stubbins: *Metall. Mater. Trans. A*, 2000, vol. 31A, pp. 2491-2502.
41. J.-K. Park, B.G. Thomas, I.V. Samarasekera, and U.-S. Yoon: *Metall. Mater. Trans. B*, 2002, vol. 33B, pp. 437-49.
42. J.-K. Park, I.V. Samarasekera, B.G. Thomas, and U.-S. Yoon: *83rd Steelmaking Conf. Proc.*, Pittsburgh, PA, March 2–29, 2000, ISS, Warrendale, PA, 2000, vol. 83, pp. 9-21.
43. O.M. Puhringer: *Stahl Eisen*. 1976, vol. 96 (6), pp. 279-84.
44. K. Miyazawa and K. Schwerdtfeger: *Ironmaking and Steelmaking*, 1979, vol. 6 (2), pp. 68-74.
45. A. Palmaers, A. Etienne, and J. Mignon: *Stahl Eisen*. 1979, vol. 99 (19), pp. 1039-50.
46. S.S. Daniel: *Ironmaking and Steelmaking*, 1982, No. 1, 16-24.
47. A. Grill and K. Schwerdtfeger: *Ironmaking and Steelmaking*, 1979, vol. 6 (3), pp. 131-35.
48. K. Miyazawa and K. Schwerdtfeger: *Arch. Eisenhuttenwes.*, 1981, vol. 52 (11), pp. 415-22.
49. F.G. Rammerstorfer, C. Jaquemar, D.F. Fisher, and H. Wiesinger: *Num. Methods in Thermal Problems*, Pineridge Press Limited, Swansea, United Kingdom, 1979, pp. 712-22.
50. T. Matsumiya and Y. Nakamura: "Mathematical Analysis of Continuously Cast Slab Bulging," Report No. 21, Nippon Steel, Chiba, Japan, 1983, pp. 347-54.
51. B. Barber, B.A. Lewis, and B.M. Leckenby: *Ironmaking and Steelmaking*, 1985, vol. 12 (4), pp. 171-75.
52. J.B. Dalin and J.L. Chenot: *Int. J. Num. Methods Eng.*, 1988, vol. 25 (1), pp. 147-63.
53. J. Gancarz, J.Y. Lamant, M. Larrecq, and P. Rahier: *74th Steelmaking Conf. Proc.*, ISS, Warrendale, PA, Washington, DC, 1991, vol. 74.
54. K. Okamura and H. Kawashima: *Proc. Int. Conf. Comp. Ass. Mater. Design Proc. Simul.*, ISIJ, Tokyo, 1993, pp. 129-34.
55. R. Mostert, R. Haardt, and K.-H. Tacke: *Steelmaking Conf. Proc.*, Baltimore, MD, ISS, Warrendale, PA, 2001, vol. 84, pp. 177-89.
56. L. Yu: Master's Thesis, University of Illinois, Urbana, IL, 2000.
57. K.-J. Lin: "Effect of Misalignment and Secondary Cooling on Bulging Strain in Continuous Cast Slabs," Report, Continuous Casting Consortium, University of Illinois, Urbana, IL, 2001.
58. Y. Sugitani, M. Nakamura, T. Kanazawa, and J.Y. Lamant: *Trans. Iron Steel Inst. Jpn.*, 1985, vol. 25, p. B9.
59. P.A. Woodberry, S.R. Story, R.B. Mahapatra, R.H. Davies, L. Moore, and R. Serje: *Steelmaking Conf. Proc.*, (Dallas, TX, March 28–31, 1993), ISS, Warrendale, PA, 1993, vol. 76, pp. 355-65.
60. K. Wunnenberg and D. Huchingen: *Stahl Eisen*. 1978, vol. 98 (6), pp. 254-59.

61. J.Y. Lamant, M. Larrecq, J.P. Birat, J.L. Hensgen, J.D. Weber, and J.C. Dhuyvetter: *Continuous Casting 85 Proc.*, Institute of Metals, London, 1985, pp. 37.1-37.8.
62. T. Matsumiya, M. Ito, H. Kajioka, S. Yamaguchi, and Y. Nakamura: *Trans. Iron Steel Inst. Jpn.*, 1986, vol. 26, pp. 540-46.
63. A. Yamanaka, K. Nakajima, and K. Okamura: *Ironmaking and Steelmaking*, 1995, vol. 22 (6), pp. 508-12.
64. Y.-M. Won, T.J. Yeo, D.J. Seol, and K.H. Oh: *Metall. Mater. Trans. B*, 2000, vol. 31B, pp. 779-94.
65. J.K. Brimacombe: *Metall. Trans. B*, 1993, vol. 24B, pp. 917-35.
66. R.A. Hardin, K. Liu, and C. Beckermann: in *Materials Processing in the Computer Age*, TMS, Warrendale, PA, 2000, vol. 3, pp. 61-74.
67. K. Dittenberger, K. Morwald, G. Hohenbichler, and U. Feischl: *VAI 7th Int. Continuous Casting Conf.*, Voest-Alpine Ind., Linz, Austria, 1996, pp. 44.1-44.6.
68. W.H. Emling and S. Dawson: *Steelmaking Conf. Proc.*, Washington, DC, ISS, Warrendale, PA, 1991, vol. 74, pp. 197-217.
69. O. Lang, C. Federspiel, M. Thalhammer, and J. Watzinger: *VAI 8th Continuous Casting Conf.*, (Linz, Austria, June 5–7, 2000), Voest-Alpine Ind., Linz, Austria, 2000, pp. 16.1-16.7.